The Arctic Ocean Perennial Ice Zone: October 1996 - May 1997

R. Kwok, G. F. Cunningham and S. Yueh

Jet Propulsion Laboratory
California Institute of Technology
4800 Oak Grove Dr
Pasadena, CA 91109

Submitted to JGR-Oceans
Nov, 1998

Corresponding author:
Ron Kwok
MS 300-235
Jet Propulsion Laboratory
4800 Oak Grove Dr
Pasadena, CA 91109
Ph. (818) 354-5614
FAX: (818) 393-3077
email: ron@rgps1.jpl.nasa.gov

The Arctic Ocean Perennial Ice Zone: October 1996 - May 1997

R. Kwok, G. F. Cunningham and S. Yueh

Abstract

We use NSCAT, RADARSAT and ice motion data to examine the perennial ice zone (PIZ) of the Arctic Ocean between Oct 1996 and May 1997. The PIZ is identified by a simple backscatter-based classification of gridded NSCAT backscatter fields. The area of the PIZ at the beginning of October occupies 5.32×10^6 km^2, approximately 76% of the Arctic Ocean ice cover. By the first of May, only 4.54×10^6 km^2 of that area remains, a decrease of 0.78×10^6 km^2 over the 7-month period. This area loss can be explained almost entirely by ice export. We estimate the ice flux through Fram Strait using ice motion derived from satellite passive microwave data. Over this period, the total area flux of sea ice through Fram Strait estimated from ice motion is 0.80×10^6 km^2, approximately 12% of the Arctic Ocean. Approximately 0.70×10^6 km^2 or 88% of the exported area is from the PIZ. Nares Strait outflow is small at 34,000 km^2, and is estimated by summing the high backscatter areas that flow out of the strait into northern Baffin Bay. After accounting for the outflow through the Fram and Nares Straits, an unexplained residual of 46,000 km^2 remains. We attribute this residual to errors in our estimation process, the unaccounted for ice flux through the Canadian Archipelago and the net divergence and convergence of the PIZ over the period. This study shows that: 1) the NSCAT backscatter fields provide an estimate of the PIZ coverage of the Arctic Ocean; and, 2) the decrease in PIZ area over the winter gives an indication of the PIZ area exported through Fram Strait.

area balance

1. Introduction

Two important physical properties that distinguish multiyear ice from first-year ice are mechanical strength and thickness. Multiyear ice is considerably stronger because of its lower brine volume and thicker because its greater age corresponds to a larger cumulative energy deficit at the surface and therefore more growth by freezing.

The climatic significance of multiyear ice coverage in the Arctic Ocean can be attributed to its strong relation to the summer ice concentration [*Comiso*, 1990; *Rothrock and Thomas*, 1990]. If there are changes in the climate which cause persistent decreases in the summer ice concentration, it would be reflected in decreases in the multiyear ice coverage in the winter. This reduction would be due to increased melt or ice export through the Fram Strait. The advection of primarily thick multiyear ice into Fram Strait represents a major source of surface fresh water for the Greenland-Iceland-Norwegian Seas, which are source regions of much of the deep water in the world's oceans [*Aagaard and Carmack*, 1989].

An accurate record of the multiyear ice coverage and its variability is therefore important in understanding the relationship between climate and multiyear ice balance. An adequate description of the sea ice cover requires the relative proportions of first-year (FY) and multiyear (MY) ice to be known as a function of time. Even though the distinction between the two ice types are relatively simple, estimates of the relative coverage of the two ice types in the Arctic Ocean have been difficult to obtain. Ice type retrieval algorithms (e.g. the Team algorithm) using satellite microwave data [*Cavalieri et al.*, 1984] have been shown [*Thomas*, 1993] to be unreliable due to the following shortcomings: 1) the retrieved MY ice fractions in the winter are much lower than the summer ice fractions and significantly lower than independent estimates [*Wittmann and Schule,* 1966; *Beaven et al.*, 1996] ; and 2) the variability in ice type fractions appear to be caused by spatial

and temporal variations in the assumed signatures. In a year-long comparison of ice type retrieval results obtained from SAR and satellite passive microwave data, *Kwok et al.* [1996] show that the SAR retrieval results produce higher and temporally less variable MY fractions over the winter. This study was however limited to the Beaufort Sea due to the unavailability of SAR data in other regions of the Arctic Ocean. *Thomas and Rothrock* [1993] used a Kalman filter/smoother to couple a physical model and the Team algorithm analyses to obtain optimal estimates of the total ice and multiyear ice fractions to overcome the inconsistencies in the temporal record. The filtering procedure increases the winter MY ice fraction and decreases the summer ice fraction to reduce the inconsistency between the summer and winter concentration estimates derived from passice microwave data. Although this consistency condition is satisfied, they note that the filtered estimates would be biased if the measurements are themselves biased.

Our contribution to the topic brings to bear three relatively new datasets: NSCAT backscatter fields of the Arctic Ocean; ice motion derived from satellite passive microwave imagery; and, synthetic aperture radar (SAR) imagery from RADARSAT. The contrast between the perennial and seasonal ice zones in the NSCAT fields are high and distinctive, thus allowing easy delineation of the two ice zone using a simple thresholding algorithm. We use the RADARSAT data and ice motion fields from passive microwave data to study and validate the temporal behavior of the derived PIZ. We show, through area balance, that the derived area of the PIZ indeed provides a reasonable estimate of the MY fraction of the Arctic Ocean over the 7-month period.

In Section 2, the three datasets used in our analysis are described. The K_u-band backscatter fields of the Arctic Ocean are new and they are synthesized directly from NSCAT observations. In Section 3, we point out the features of the ice cover that can be observed in these time-sequential fields between October 1996 and May 1997. Even though the spatial resolution of the data is fairly coarse, the coverage of the data and the

stability of the backscatter over the 7-month period are valuable for inferring changes in the ice cover. Section 4 describes the objective procedure for identification of the perennial ice zone (PIZ) in the NSCAT fields. In Section 5, we analyze the temporal behavior of the PIZ area within the Arctic Ocean by considering the convergence/divergence of the PIZ and the export of PIZ area through different passages out of the Arctic Ocean. The decrease in area of the PIZ over the 7-month period is explained, to within the uncertainty in the estimates, by ice export and ice cover deformation. Our time series of PIZ area are compared to MY ice coverage derived from passive microwave fields and model estimates from other investigations. The last section summarizes the paper.

2. Data Description

NSCAT backscatter fields. NSCAT is a K_u-band scatterometer on board the Japanese ADEOS platform. The primary mission of this instrument is to measure wind over the ocean surface. The scatterometer uses six fan beam antennas illuminating two 600 km swaths on each side of the spacecraft ground track [*Naderi et al.*, 1992]. The fore- and aft-antennas operate at vertical polarization, while the mid-beam antennas can transmit and receive vertically or horizontally polarized radiation. The data have a spatial resolution of 7 km × 25 km after radar processing. For consistent wind estimates, the backscatter measurements are calibrated to better than 0.25 dB.

The fields of normalized backscatter of the Arctic Ocean created here (Plate 1) are sampled on a 12.5 km by 12.5 km SSM/I polar stereographic grid. The near-simultaneous NSCAT measurements from all the antenna beams are combined to estimate the 50° incidence angle backscatter at each grid point. To do this, we assume a linear relation [*Yueh et al.*, 1997],

$$\sigma_o(\theta) = A + B(\theta\text{-}50) \text{ dB}$$

between backscatter, σ_o, and incidence angle, θ (in degrees). Available measurements for determining the regression coefficients *A* and *B* are weighted by the fractional area of NSCAT resolution cells falling inside the 12.5 km × 12.5 km grid cells. Each backscatter field is constructed from data accumulated from approximately three days of NSCAT coverage of the Arctic Ocean. Results from a simple and effective ice/open ocean classifier are used to mask out areas of open water (colored blue in Plate 1). In this algorithm, a pixel is classified as sea ice if *A* is between -25 dB and 0 dB and the mid-beam polarization ratio (VV/HH) is between -3 and 2 dB. Otherwise, it is classified as open water. Details of these algorithms can be found in *Yueh et al.*, [1997] and *Yueh and Kwok* [1998].

RADARSAT Images. The Synthetic Aperture Radar (SAR) data used here are processed and archived at the Alaska SAR Facility (ASF) in Fairbanks. The RADARSAT C-band imaging radar transmits and receives horizontally-polarized radiation (HH). The imagery used here (resolution ~ 150 m) are collected by the radar operating in one of its multi-beam modes which illuminates a 460 km wide ground swath. The incidence angle within the swath varies over a range of 20° to 44°. The data from the ASF SAR processor have an absolute calibration accuracy of 2 dB and a relative calibration accuracy of 1 dB.

SSM/I Ice Motion. The 1-day ice motion fields are derived from sequential Special Sensor Microwave Imager (SSM/I) brightness temperature fields. Procedures used to construct these motion fields are described in *Kwok et al.* [1998]. Individual motion vectors are expected to have uncertainties of 5-6 km/day. Uncertainties in average ice motion over a longer time period are lower since the error statistics are normally distributed.

3. NSCAT backscatter fields

NSCAT was operational between September 1996 and June 1997. For this study, we constructed 90 backscatter fields of the Arctic Ocean spanning the period between fall

freeze-up and onset of melt in the spring. A subset of the fields that illustrate the time-dependent backscatter behavior of the ice cover are shown in Plate 1. In this section, we provide somewhat qualitative observations of the backscatter time-series which are treated in more detail in the following sections.

The time-series shows a significant backscatter contrast (4-7 dB) between the perennial ice zone (PIZ) and the zone of seasonal ice (SIZ) that is persistent throughout the year. The PIZ is mostly covered by multiyear (MY) ice whereas the primary ice type in the SIZ is first-year (FY) ice. The scattering from the inhomogeneities in the low salinity MY ice volume, snow grains, hummocks and ridges within an NSCAT resolution element give the ice cover a characteristic high backscatter. The FY ice cover has a lower backscatter because this higher salinity ice type causes surface backscatter to be the dominant component of the radar return. The backscatter level within the two zones remain remarkably stable throughout the season. Growth in the area of the SIZ (low backscatter regions) over the winter is evident over the 7-month sequence. The areal coverage of FY ice in the SIZ is small at the end of summer but increases rapidly after fall freeze-up. Over the winter, there is a slow decrease in the PIZ coverage of the Arctic Ocean. Animation of the time sequence of NSCAT backscatter fields suggests export of high backscatter PIZ ice through Fram Strait. The East Greenland Current carries this ice south toward the Denmark Strait. In the East Greenland Sea, the areal coverage of the high backscatter ice from the Arctic Ocean PIZ increases quickly at first but slows after mid-January. The Odden ice tongue in the Greenland Sea which failed to develop during both 1994 and 1995, is noticeable from mid-November through early April although it is not clear whether any of the older ice is advected into the ice tongue. There is no visually observable outflow of sea ice from the PIZ through the Bering Strait or the passages into the Barents and Kara Seas. Outflow through the Nares Strait is evident in the animation. High backscatter ice drifting through the strait are periodically 'calved' off of the ice area near the southeast coast of Ellesmere Island.

We use this dataset to study the evolution of the area of the PIZ from October 1996 through May 1997. To determine whether this dataset is useful quantitatively, we pose the following questions: Can we define the boundaries of the PIZ objectively over the study period?; Is the backscatter of the PIZ stable throughout the season?; and, Can the change in area of the PIZ in the Arctic Ocean be explained by ice export and convergence/divergence of the ice cover? The answer to the last question allows us to decide whether our analysis provides a quantitative description of the PIZ coverage of the Arctic Ocean.

4. Definition of the Perennial Ice Zone (PIZ)

We analyze the area of the PIZ within the boundaries of the Arctic Ocean domain shown in Fig. 1. The area of the PIZ is defined as the sum of the area of all pixels above a certain backscatter threshold. The estimation of this threshold is discussed below.

4.1 Time-dependent threshold

The large spatial gradient in backscatter in the transition region between the perennial and seasonal ice zones provides a clear definition of the edge of the PIZ. Fig. 2 shows this transition region in an NSCAT backscatter field and a coincident RADARSAT image. The -12 dB and -13 dB NSCAT backscatter isopleths are overlaid on both images. Although there is a large disparity between the resolution of the two sensors, the correlation in the spatial and radiometric content between the datasets are good. Fig. 3 shows the backscatter values of ice mixtures (MY and FY ice) in the SIZ and PIZ from four RADARSAT/NSCAT image pairs. By definition, MY ice is the principal ice type in the PIZ whereas FY ice is the principal ice type in the SIZ. These results show that the C-band contrast between the two ice zones is approximately 2 to 3 dB, while the higher contrast at K_u-band ranges from 4 dB to more than 7 dB. The contrast at C-band is slight lower than that observed by *Kwok and Cunningham* [1992] because of the mixing

deformed and undeformed ice over the large areas are sampled here. In their paper, the backscatter of relatively pure MY and FY areas are studied. This higher contrast in the NSCAT data allows us to unambiguously identify the boundary between the ice zones. Other investigators [*Long and Drinkwater*, 1999; *Remund et al.*, 1998] have also exploited this distinctive contrast in the K_u-band data to extract information relating to ice type and ice extent.

The enhanced K_u-band contrast of PIZ and SIZ ice at 50° incidence over that C-band can be explained as follows. For low-salinity MY ice, we believe enhanced contribution of volume scattering from the inhomogeneities increases backscatter at the shorter K_u-band wavelength. The lower K_u-band backscatter of FY ice is probably due to a further decrease in the volume scattering contribution to the total radar return as a result of decreased penetration. Moreover, lower backscatter from FY ice at the higher incidence angle NSCAT measurements is expected.

We employ the following procedure to obtain an objective estimate of the backscatter threshold to determine the PIZ area. The average of the backscatter values at the locations of maximum gradient over an NSCAT backscatter field is selected as the threshold for that image. Vector gradients are computed by taking the central differences (separation = 50 km) along two orthogonal axes defined by the image coordinate system. A plot of these backscatter thresholds sampled twice a month (Fig. 4) shows a time-dependent trend, ranging from approximately -12 dB in early October to -13 dB in May. The standard deviation is 0.27 dB. This trend is unexpected. In order to eliminate the possibility of a slow drift in the NSCAT sensor calibration, we examine the time-dependence of the K_u-band backscatter of a 30,000 km^2 area in Northeast Greenland that is above the 2 km elevation contour. The backscatter from this cold, low accumulation, dry snow zone should remain very stable during the winter. Indeed over the winter, the trend in backscatter is negligible (within the calibration accuracy of 0.25 dB) compared to the more

than 1 dB decrease over the sea ice cover within the PIZ (Fig. 5). It is important to note here that this decrease in backscatter is not a local effect, as it is observed over the entire PIZ ice cover. Based on the above results, we conclude that this trend is probably a natural phenomenon (discussed in more detail below) and not likely to be a measurement artifact. Hence, the coefficients from regression of the measured threshold against time are used to determine the linear time dependent thresholds used in computing the PIZ area.

Two sources of error affect the uncertainty in the PIZ area: 1) the variability of the thresholds (0.26 dB); and 2) the effect of calibration of the backscatter measurements (0.25 dB) on threshold determination. Together they introduce an uncertainty of approximately 106,000 km^2 or 1.8% in the determination of the PIZ area.

To obtain a more quantitative description of the MY fraction one expects to find within the PIZ, we use RADARSAT imagery to estimate the MY ice fraction just within this PIZ boundary. The MY ice fraction is determined using a simple classifier outlined in *Kwok et al.* [1992]. From four coincident NSCAT and RADARSAT images, we find that the MY fraction within 100 km of the PIZ boundary to be between 0.90 and 0.94. We expect that the MY fraction in the interior of the PIZ to be higher.

4.2 Decrease in backscatter over the 7-months

This decrease in backscatter over such a large area of the ice cover is interesting. Net divergence would introduce lower backscatter ice into PIZ thus reducing its average backscatter. However, it is unlikely that net divergence could alone account for this magnitude of backscatter decrease. Assuming a linear mixing of the normalized backscatter power of MY(P_{MY}) and FY (P_{FY}) ice, the total observed power at the radar, P_{tot}, is given by,

$$P_{tot} = \alpha P_{MY} + (1 - \alpha) P_{FY}$$

where α is the MY fraction. The average backscatter of the sea ice within the PIZ and SIZ are approximately -8 dB and -15 dB. These are obtained by averaging the backscatter of the sea ice within the PIZ and the SIZ. This gives a ratio of P_{MY}/P_{FY} of 5.0. With a large MY fraction, higher backscatter MY ice dominate the observed backscatter. It would take a large increase in the areal coverage of FY ice to affect P_{tot}. For example, more than a 30% net divergence of the PIZ ice cover is required to reduce the observed backscatter by 1 dB. We also show in the next section that the net divergence/convergence within the PIZ is probably quite small (1-2%).

We speculate that this trend in the backscatter might be related to snow cover, more specifically, to changes at the snow ice interface. It is unlikely that the snow cover will have a large effect because the attenuation of cold, dry snow at K_u-band is negligible. At the end of the summer, the surface of the ice cover is relatively bare. Snow accumulation over the surface and the changes of the snow ice interface during the winter would have a more definite effect on the scattering properties of the ice cover. For a decrease in backscatter to occur, the changes at the snow ice interface would have to reduce the contribution of scattering from the ice volume thus reducing the overall backscatter of the older ice. We are not, however, aware of any studies in the published literature detailing the evolution of the physical properties of the snow ice interface over the winter.

5. Area Balance of the PIZ

The area of the PIZ from October 1996 through May 1997 is shown in Fig. 6. At the beginning of November, the area of the PIZ is approximately 5.32×10^6 km^2 occupying approximately 76% of the Arctic Ocean. By the first of May, the remaining area is 4.54×10^6 km^2, a loss of 0.78×10^6 km^2 over the 7 month period. The variability in the PIZ area superimposed on the downward trend is 62,000 km^2, is approximately 1.3% of the average PIZ area. The boundaries of the PIZ at the beginning of October, 1996 and May,

1997 (Fig. 1) show the westward advection of ice due to the Beaufort Gyre and the northward motion of the PIZ edge in the Eurasian Basin.

In this section, the area loss from the PIZ is examined. If we consider the area balance of the PIZ within the Arctic Ocean domain to be affected by only export and deformation, then the area of the PIZ at time t can be written as,

$$A_{PIZ}(t) = A_{PIZ}(0) - (A_{export}(t) + A_{def}(t)).$$

A_{export} is the export of PIZ area through the different passages in the Arctic Ocean and A_{def} is the area change of the PIZ due to convergence and divergence from ridging or opening of leads. Net melt of MY ice is assumed to be zero, a reasonable assumption in the winter Arctic Ocean.

5.1 Ice Export

The passages out of our Arctic Ocean domain bordering the PIZ are Fram Strait, Nares Strait and the openings into the Canadian Archipelago. There is no visually observable outflow of sea ice from the PIZ through the Bering Strait and the passages into the Barents and Kara Seas, so the PIZ ice flux through these passages are not considered here.

Fram Strait

We estimate the area flux of ice through Fram Strait using the technique described in *Kwok and Rothrock* [1998]. Briefly, daily ice motion over an area of approximately 780 km x 780 km centered around Fram Strait is derived from sequential SSM/I 85 GHz V records over the 7-month period. The area flux is estimated at a gate positioned on a 400 km line, roughly along 81°N, drawn across the passage between Antarctic Bay in northeast Greenland and the northwestern tip of Svalbard. Ice export is estimated by integrating the ice motion over twenty sample points along the flux gate using the simple trapezoidal rule.

Ice area export through Fram Strait should be the largest component of the A_{export} term in the area balance. Fig. 7 shows the area flux through Fram Strait between October 1996 and May 1997. The total ice area exported over the seven months is 797,000 km^2. The uncertainty in this ice flux estimates is approximately 4% of the total area flux [*Kwok and Rothrock*, 1998].

To estimate only the PIZ component of this outflow, we weigh the cross-strait velocity profile by the PIZ pixels crossing the flux gate. Over 88% of the total area flux is from the PIZ. This results in a PIZ export through the Fram Strait of about 697,000 km^2. The average backscatter profile of the sea ice along the flux gate is shown in Fig. 8. The high backscatter ice in the western part of Fram Strait is from the PIZ in the Arctic Ocean and has large MY ice fractions while the lower backscatter seasonal ice has come westward across the north of Svalbard from the Arctic Ocean north of the Barents and Kara Seas.

Nares Strait

Animation of the NSCAT backscatter fields reveals an outflow of ice through the Nares Strait between the Northwest coast of Greenland and Ellesmere Island. Fig. 9 shows an NSCAT backscatter field and a coincident RADARSAT image of the opening into Nares Strait (approximately 30 km wide) in the Arctic Ocean. The high resolution SAR image shows the characteristic 'arch' feature, also evident in the NSCAT data, formed from leads at the opening into this narrow passage. Note that the perennial pack does not move through the strait as an unbroken ice cover. Rather, leads form in the perennial pack as floes are broken off the 'arch' and transported through the passage. This causes the Nares Strait sea ice outflow into Baffin Bay to have a larger fraction of FY ice. In the lower resolution NSCAT fields, the evidence of outflow is apparent in both the periodic appearances of low backscatter features (the arch) in the ice cover in the Lincoln Sea and flows of ice with backscatter characteristic of the PIZ out of Nares Strait into northern

Baffin Bay (see Plate 1). However, a direct measurement of the ice motion into the Nares Strait cannot be made in the same manner as in the Fram Strait. This passage is too small compared to the resolution of the 85 GHz passive microwave data. Our approach is to measure the outflow at the opening of Nares Strait into Baffin Bay.

The NSCAT fields show relatively large areas of ice clearly flowing from Nares Strait into upper Baffin Bay with backscatter values similar to that in the PIZ. We compute the ice area within a spatial window using the thresholds defined above. The area of the PIZ ice in this region is shown Fig. 10. Note that the defined region excludes any possible outflow of PIZ ice from Lancaster Sound. The results show that there are periodic episodes of higher areal coverage. Examination of the animation reveals that the maxima in the plots coincide with times when large areas of bright ice appear to be 'calved' from the mouth of the Strait and move southward into Baffin Bay. Summing the areas at these peaks then gives us an estimate of the total ice area transported through Nares Strait. Note that the earliest peak in early October corresponded to high backscatter sea ice entering the region from the southeast and is therefore ignored. However, the double peak in early March though near to each other in time, does represent separate flows of bright ice when viewed in the animation.

The seven identified peak events are measured above a background value, which appears to include PIZ ice along the Southeast coast of Ellesmere Island. Summing these values results in a total ice flux of 75,300 km^2 with an associated uncertainty of 17% due to 0.25 dB in calibration accuracy. However, the mean backscatter of the ice exiting into Baffin Bay is 2.7 dB lower in backscatter than the PIZ ice measured in the Lincoln Sea. This decrease is due to mixing of PIZ ice with FY ice formed in the Strait. We use the mixture model described above to estimate the MY fraction of the ice exiting the Strait. The seasonal ice found in upper Baffin Bay has a mean backscatter of -15.2 dB with a standard deviation of 0.67 dB while the perennial ice in the Lincoln Sea has a mean

backscatter of -7.3 dB with a standard deviation of 0.24 dB. A perennial ice fraction of 0.45 results if these values are used. Accounting for these factors, we estimate an export of PIZ area through the Nares Strait of about 34,000 km^2 with an uncertainty of 26%.

5.2 Deformation of PIZ

Divergence and convergence of the PIZ ice cover would add or subtract from the total area of the PIZ area. We use SSM/I ice motion fields to obtain an estimate of the net divergence/convergence of the interior of the PIZ. A polygon is used to define an initial area interior to the edge of the PIZ such that this area stays within our Arctic Ocean domain through May 1, 1997. It is the deformation of the PIZ area within our domain that is of interest. We do not extend the polygon beyond the edge of the PIZ because of the lack of good motion data in some of these regions. On Oct 1, 1996, the vertices of this polygon are located on the points of a uniformly-spaced ice motion grid (100 km by 100 km). The initial polygon vertices are selected based on the location of these vertices on May 1, 1997. We require that these vertices to remain within our domain over the 7-month period. The trajectories of each point is estimated using 1-day ice motion fields derived from sequential SSM/I data. Fig. 11 shows the polygon at the beginning and end of the 7-month period. The final shape of the polygon seems to give a fair characterization of the motion and deformation of the PIZ interior compared to the boundaries of the PIZ.

Fig. 12 shows the area of the polygon and PIZ area over the period. The initial area of the polygon is approximately 3.25×10^6 km^2. At the end of the 7-months, there is a net increase in area of 48,000 km^2, or 1.4% of the initial area. After detrending, the polygon area exhibits a variability of 25,000 km^2, or only 0.8%. This variability is much smaller compared to the variability of the PIZ area of 62,000 km^2. Correlation of the detrended PIZ area and area of the polygon gives $R = 0.55$. This shows reasonable correspondence between the ice motions predicted deformation and the derived PIZ area.

Since the ice area within the interior of the PIZ appears to be changing little as a whole, the PIZ area exterior to the polygon must explain most of this variability. The correlation of the detrended PIZ area outside the polygon and the PIZ area gives R=0.94. The changes in the PIZ area outside the polygon explains more than 88% of the variance of the PIZ area. This is not a surprising result since we expect the interior MY pack to deform little during the winter.

The above exercise gives us an estimate of only the net area change and the variability of the PIZ within the polygon. We do not, however, have an estimate of the $A_{def}(t)$ term for the entire PIZ ice cover. If we assume that 1.4% is an indication of net divergence of the ice cover, then the net area increase of the ice cover over the 7-month period would be 78,500 km^2. This quantity, however, may not be indicative of the net divergence of the ice cover. We note that compared to the natural variability of the PIZ area of 1.3%, the 1.4% trend in the divergence computed here may not be significant. For example, the convergence of the ice cover north coast of Greenland and Canadian Archipelago could easily reduce the total area change to zero. So, for the area balance computation here, we left it as an unknown.

5.3 Discussion of Area Balance

Table 1 shows the area balance at the beginning of May, 1997. Using the available estimates for terms in the PIZ area balance and their associated uncertainty, we are left with a residual of approximately 46,000 km^2 with an uncertainty of 111,000 km^2 on the first of May, 1997. The uncertainty in this estimate is much larger than the mean and is dominated by the errors in the calculation of the PIZ area due to two factors mentioned above: 1) the determination of the thresholds; and, 2) the calibration accuracy of the sensor. The decrease in area of the PIZ over the period can be explained almost entirely by ice export through Fram Strait.

In the area balance, we have neglected outflow of the PIZ area into the Canadian Archipelago and the net deformation of the PIZ area is left as an unknown. The outflow of PIZ ice through flux gates into the Canadian Archipelago is likely to be smaller than the uncertainty in the final estimates. If there is net divergence or convergence of the PIZ area, it would increase the unaccounted for PIZ ice area. Net divergence would give a positive residual and indicate that export of the PIZ area is underestimated whereas net convergence indicates otherwise. A net divergence or convergence of 1% contributes approximately 50,000 km^2 to the imbalance. If indeed the net convergence/divergence of the PIZ ice cover is of the order of only 1-2% , then the unaccounted for area would change by the same amount.

5.4 Comparison with passive microwave retrievals

Finally, we compare our PIZ area with the MY coverage of the Arctic Ocean derived from the SSM/I data. These datasets are archived at the National Snow and Ice Data Center (NSIDC). Fig. 13 shows the ice area within our Arctic Ocean domain covered by more than 80%, 60% and 30% concentration of MY ice. Several features are evident: 1) our PIZ area estimates correspond to approximately the 30% coverage curve; 2) the variability of the two time series are correlated - with the SSM/I derived data having the higher of the two; and, 3) both time-series exhibit a downtrend over the 7-month period.

Based on our comparison with high-resolution RADARSAT imagery and assuming an average MY ice concentration of 90% within the PIZ, we estimate that 68% of the Arctic Ocean is covered by MY ice on Oct 1, 1996. The passive microwave derived dataset gives a MY coverage of around 49%, significantly lower than our estimates. The underestimation of MY ice coverage by this dataset and the possible causes has been noted by a number of investigators [*Thomas*, 1993; *Beaven et al.*, 1996; *Kwok et al.*, 1996]. Perhaps a better comparison would be with the results of a filtering scheme

described in *Thomas and Rothrock* [1993] and *Thomas et al.*[1996]. In their work, a Kalman filter/smoother blends the results from a physical model with SSM/I derived ice type and concentration to obtain more consistent estimates of total ice and multiyear ice fractions. Their results show, over the period from 1979 through 1985, that on the average 60% of the area of Arctic Ocean is covered by MY ice. These estimates are more comparable with our results.

Other than the bias in the MY retrievals in the NSIDC dataset, the correlation between the variability and the downtrend are interesting. We expect that the shorter wavelength passive microwave measurements to be more sensitive to changes in the ice cover thereby giving the time-series higher variability. The temporal variability may not be related to changes in the true concentration. The downtrend in the PIZ area, which can be explained almost entirely by ice export through the Fram Strait, can also be seen in the passive microwave data although this trend is masked by the noisier MY area time-series from the passive microwave data.

6. Conclusions

We have shown, through area balance, that we can obtain an estimate of the coverage of the perennial ice zone using backscatter fields from the NSCAT K_u-band scatterometer. RADARSAT and ice motion data are used to understand the trend and the variability of the behavior of the PIZ area over the 7-month period. The quality and coverage of the NSCAT data, and the stability of the backscatter of the ice cover are valuable for studying the ice cover.

The interesting results are:

1. The PIZ area at the beginning of October, 1996 occupies 5.32×10^6 km^2, approximately 76% of the Arctic Ocean ice cover. Or, multiyear ice covers 68% of the Arctic Ocean assuming a 90% MY concentration within the PIZ.

2. By the first of May, only 4.54×10^6 km^2 of that area remains, a decrease of 0.78×10^6 km^2 over the 7-month period.
3. This area loss can be explained almost entirely by ice area flux through Fram Strait. Over this period, the total area flux of sea ice through Fram Strait is 0.80×10^6 km^2, approximately 12% of the Arctic Ocean. Approximately 0.70×10^6 km^2 or 88% of that area is exported from the PIZ. A large fraction of the exported ice is from the perennial ice zone.
4. We estimate the PIZ area exported through Nares Strait to be 46,000 km^2.
5. After accounting for the outflow through the Fram and Nares Straits, an unexplained residual of 46,000 km^2 remains. We attribute this residual to errors in our estimation process, the unaccounted for ice flux through the Canadian Archipelago and the net divergence and convergence of the PIZ over the period.
6. The PIZ derived from Ku-band scatterometer data provides an estimate of the MY ice coverage of the Arctic Ocean; the decrease in its area over the winter is an indicator of the ice area flux through the Fram Strait. Future K_u-band scatterometers (e.g. QUIKSCAT) provide another dataset for monitoring the Arctic sea ice cover.

Acknowledgments

The SSM/I data brightness temperature fields are provided by World Data Center A for Glaciology/National Snow and Ice Data Center, University of Colorado, Boulder, CO. The RADARSAT data are provided by the Alaska SAR Facility, Fairbanks, AK. R. Kwok, G. F. Cunningham and S. Yueh performed this work at the Jet Propulsion Laboratory, California Institute of Technology under contract with the National Aeronautics and Space Administration.

References

Aagaard, K., and E. Carmack, The role of sea ice and other fresh water in the Arctic circulation, *J. Geophys. Res. 94*(C10), 14,485-14,498, 1989.

Beaven, S. G., S. Gogineni and F. D. Carsey, Fusion of satellite active and passive microwave data for sea ice type concentration estimates, *IEEE Trans. Geosci. Remote Sens.*, 34(5), 1172-1183, 1996.

Cavalieri, D. J., P. Gloersen and W. J. Campbell, Determination of sea ice parameters from Nimbus 7 SMMR, *J. Geophys. Res.*, 89(D4), 5355-5369, 1984.

Comiso, J. C., Arctic multiyear ice classification and summer ice cover using passive microwave satellite data, *J. Geophys. Res.*, 95(C8), 13411-13422, 1990.

Kwok, R. and D. A. Rothrock, Variability of Fram Strait ice flux and North Atlantic Oscillation, *J. Geophys. Res.*, in press.

Kwok, R., A. Schweiger, D. A. Rothrock, S. Pang and C. Kottmeier, Sea ice motion from satellite passive microwave data assessed with ERS SAR and buoy data, *J. Geophys. Res.*, 103(C4), 8191-8214, 1998.

Kwok, R., J. C. Comiso and G. F. Cunningham, Seasonal characteristics of the perennial sea ice cover of the Beaufort sea, *J. Geophys. Res.*, 101 (C12), 28417-28439, 1996.

Kwok, R and G. F. Cunningham, Backscatter Characteristics of the Winter Sea Ice Cover in the Beaufort Sea, *J. Geophys. Res.*, 99 (C4), 7787-7803, 1994.

Kwok, R., E. Rignot, B. Holt and R. G. Onstott, Identification of sea ice type in spaceborne SAR data, *J. Geophys. Res.*, 97 (C2), 2391-2402, 1992.

Long, D. G. and M. Drinkwater, Cryosphere Applications of NSCAT data, *IEEE Trans. Geosci. Remote Sens.*, in press.

Naderi, F. M., M. H. Feilich and D. G. Long, Spaceborne radar measurements of wind velocity over the ocean - An overview of the NSCAT scatterometer system, *Proc. IEEE* , 79(6), 850-866, 1991.

Remund, Q. P., D. G. Long and M. R. Drinkwater, Polar sea ice classification using enhanced resolution NSCAT data, *Proc. of IGARSS*, Seattle, Washington, 1998.

Thomas, D. R., Arctic sea ice signatures for passive microwave algorithms, *J. Geophys. Res.*, 98(C6), 10037-10052, 1993.

Thomas, D., S. Martin, D. Rothrock and M. Steele, Assimilating satellite concentration data into an Arctic sea ice mass balance model, 1979-1985, *J. Geophys. Res.*, 101(C9), 20849-20868, 1996.

Thomas, D.R. and D. A. Rothrock, The Arctic Ocean ice balance: A Kalman filter smoother estimate, *J. Geophys. Res.*, 98 (C6), 10053-10067, 1993.

Wittmann, W. I. and J. Schule Jr., Comments on the mass budget of Arctic ice pack, *Proceedings of the Symposium on the Arctic Heat Budget and Atmospheric Circulation*, J. O. Fletcher, ed., 215-246, Memo. RM-5233-NSF, Rand Corp., Santa Monica, CA, 1966.

Yueh, S., R. Kwok, S. H. Lou and W. Y. Tsai, Sea ice identification using dual-polarized Ku-band scatterometer data. *IEEE Trans. Geosci. Remote Sens.* 35(3), 560-569, 1997.

Yueh, S. and R. Kwok, Arctic sea ice extent and melt-onset from NSCAT observations, *Geophys. Res. Lett.*, in press, 1998.

Figure Captions

Figure 1. The Arctic Ocean domain. Also shown are the boundaries of the PIZ on Oct 1, 1996 and May 1, 1997.

Figure 2. RADARSAT SAR imagery and NSCAT backscatter field showing the transition between the PIZ and SIZ (time, date). Backscatter isopleths (-12 dB and -13 dB) on the RADARSAT image are derived from the co-located NSCAT backscatter field.

Figure 3. Average backscatter over seasonal and perennial ice areas (Sample area ~ 5,000 km^2) extracted from four RADARSAT/NSCAT image pairs.

Figure 4. Trend of backscatter thresholds used to determine the area of the PIZ.

Figure 5. Comparison of the mean backscatter of an area over Northeast Greenland and the backscatter within the PIZ as defined by the time-varying thresholds in Fig. 4.

Figure 6. PIZ area over the 7-month period; sum of the PIZ area and the area flux through Fram Strait derived from satellite passive microwave ice motion. Dashed lines indicate the uncertainty in the determination of the PIZ area due to calibration and uncertainty in threshold estimates.

Figure 7. Total ice, PIZ ice and SIZ ice area flux through the Fram Strait estimated using ice motion and NSCAT backscatter fields.

Figure 8. Average backscatter profile of sea ice across Fram Strait.

Figure 9. Coincident NSCAT and RADARSAT images of the Nares Strait.

Figure 10. PIZ ice area computed within a region south of the Nares Strait.

Figure 11. Deformation of a polygon defined within the PIZ boundaries. (a) Oct 1, 1996; (b) May 1, 1997.

Figure 12. Comparison of (a) polygon area inside PIZ; (b) PIZ area.

Figure 13. Comparison of PIZ area with Arctic Ocean MY ice area coverage and ice area covered by more than 80%, 60% and 30% concentration of MY ice; MY concentrations derived from satellite passive microwave brightness temperature.

Plate 1. Sample of NSCAT backscatter fields from Oct 1, 1996 through May 1,1997.

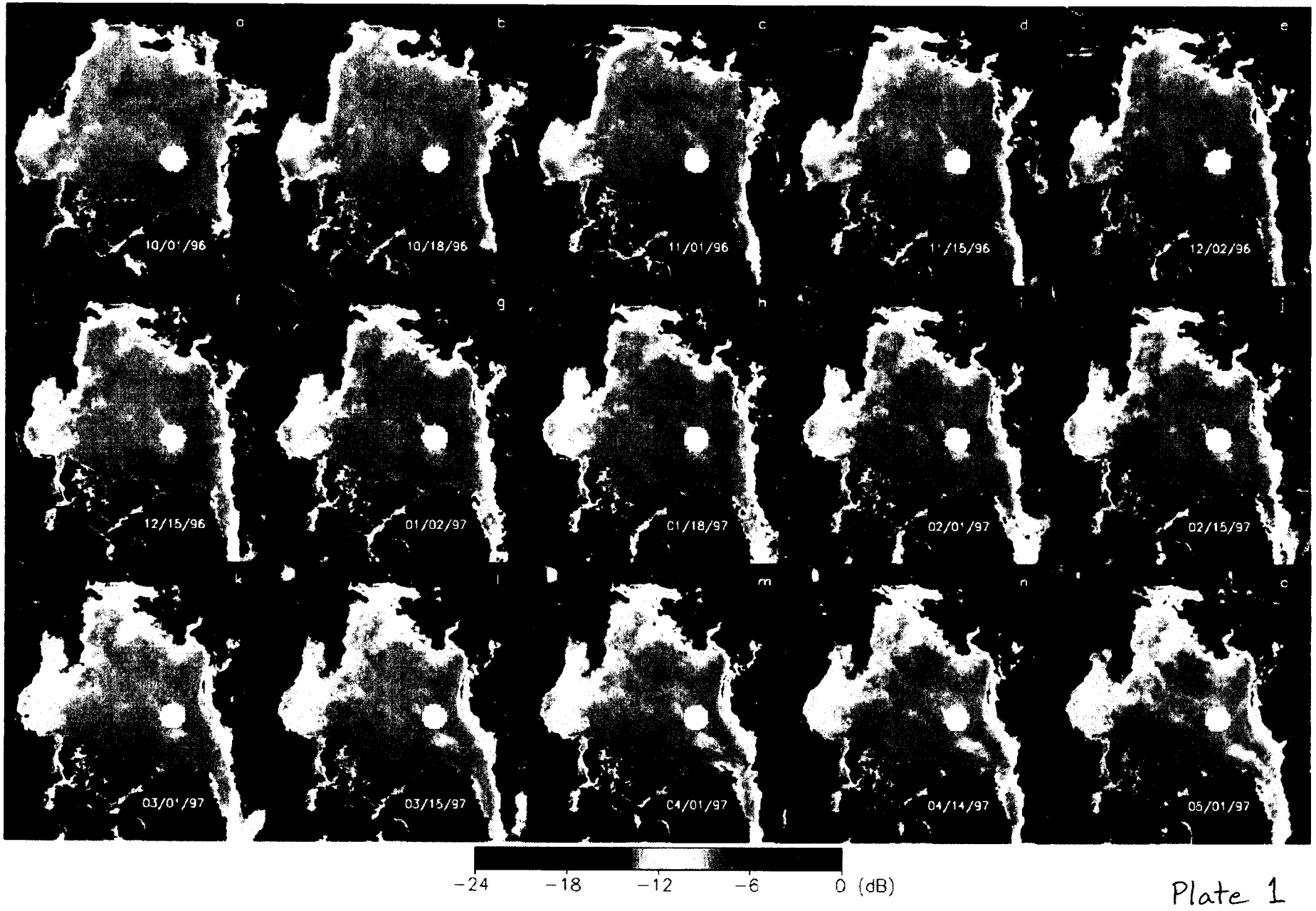
a
10/01/96
b
10/18/96
c
11/01/96
d
11/15/96
e
12/02/96
f
12/15/96
g
01/02/97
h
01/18/97
i
02/01/97
j
02/15/97
k
03/01/97
l
03/15/97
m
04/01/97
n
04/14/97
o
05/01/97
−24
−18
−12
−6
0 (dB)

Plate 1

Fig. 1

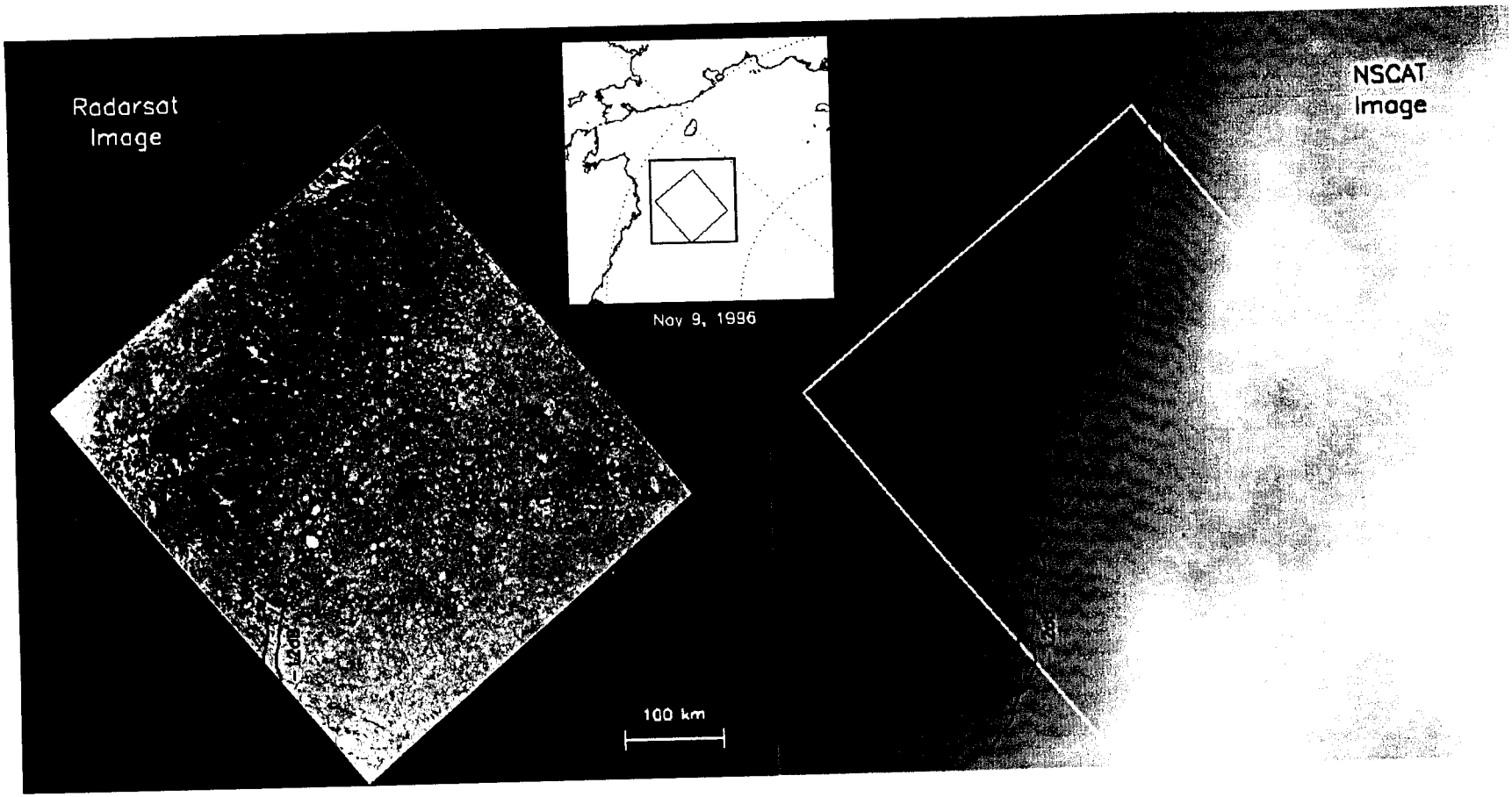

Fig. 2

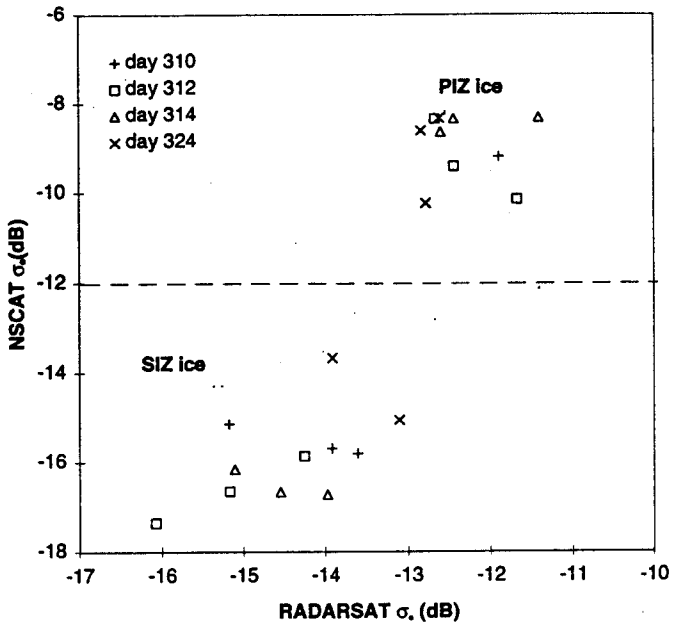
+ day 310
□ day 312
△ day 314
× day 324
PIZ ice
SIZ ice
-6
-8
-10
-12
-14
-16
-18
-17
-16
-15
-14
-13
-12
-11
-10
NSCAT σ₀(dB)
RADARSAT σ₀ (dB)

Fig. 3

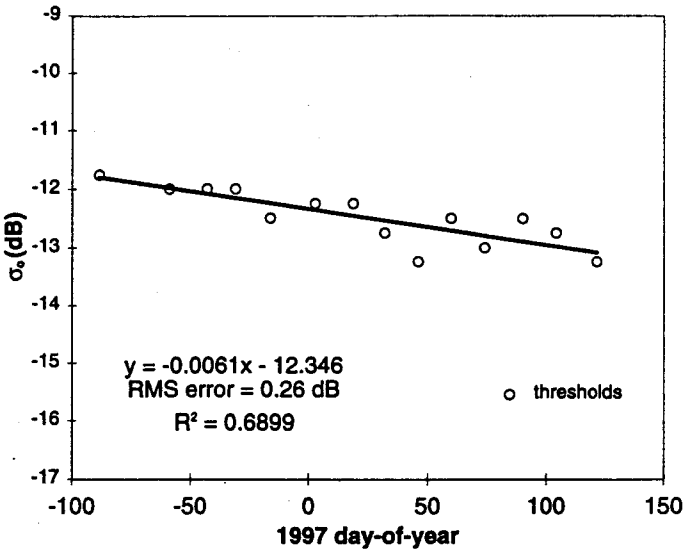
-9
-10
-11
-12
-13
-14
-15
-16
-17
σ_o (dB)
y = -0.0061x - 12.346
RMS error = 0.26 dB
R^2 = 0.6899
thresholds
-100
-50
0
50
100
150
1997 day-of-year

Fig. 4

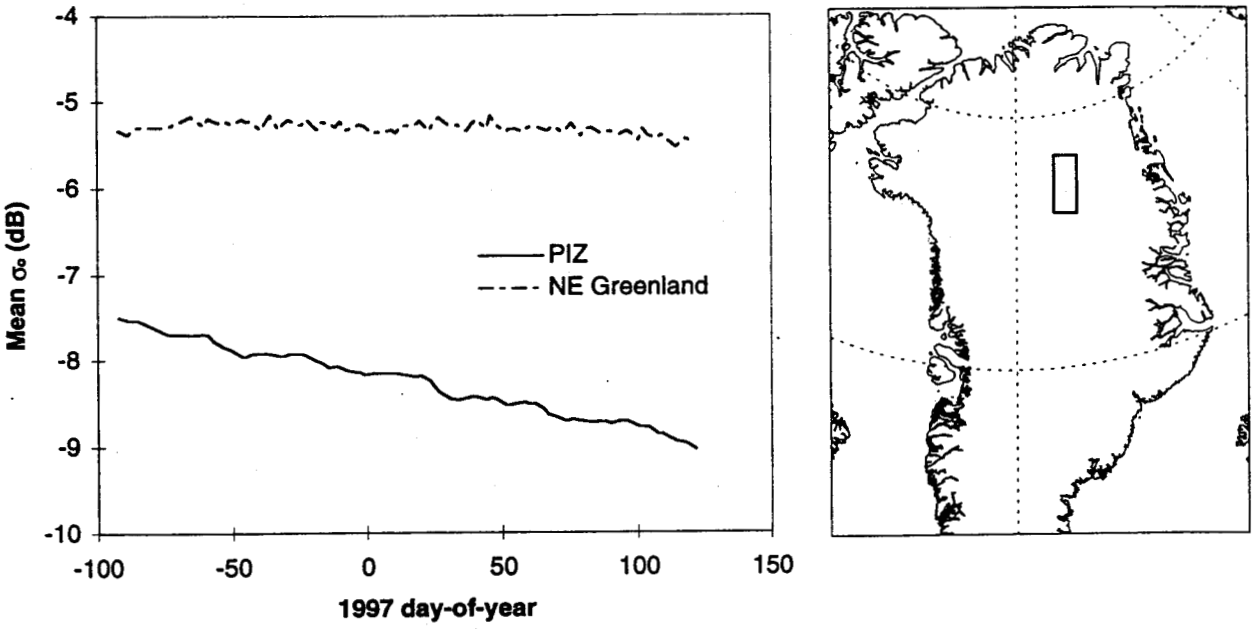
-4
-5
-6
-7
-8
-9
-10
Mean σ₀ (dB)
PIZ
NE Greenland
-100
-50
0
50
100
150
1997 day-of-year

Fig. 5

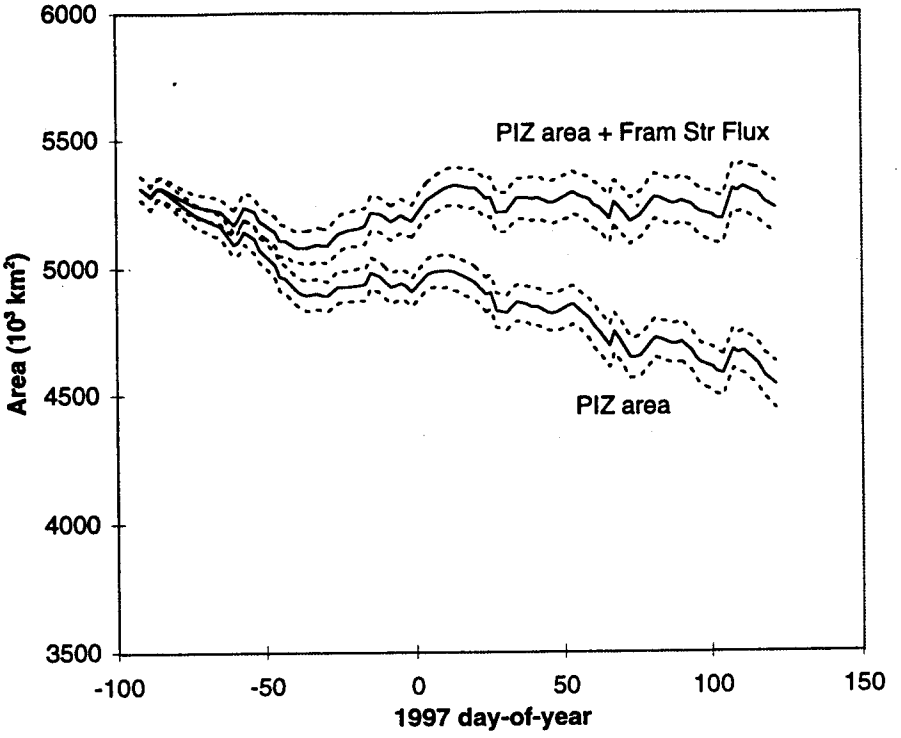
6000
5500
5000
4500
4000
3500
Area (10^3 km^2)
PIZ area + Fram Str Flux
PIZ area
-100
-50
0
50
100
150
1997 day-of-year

Fig. 6

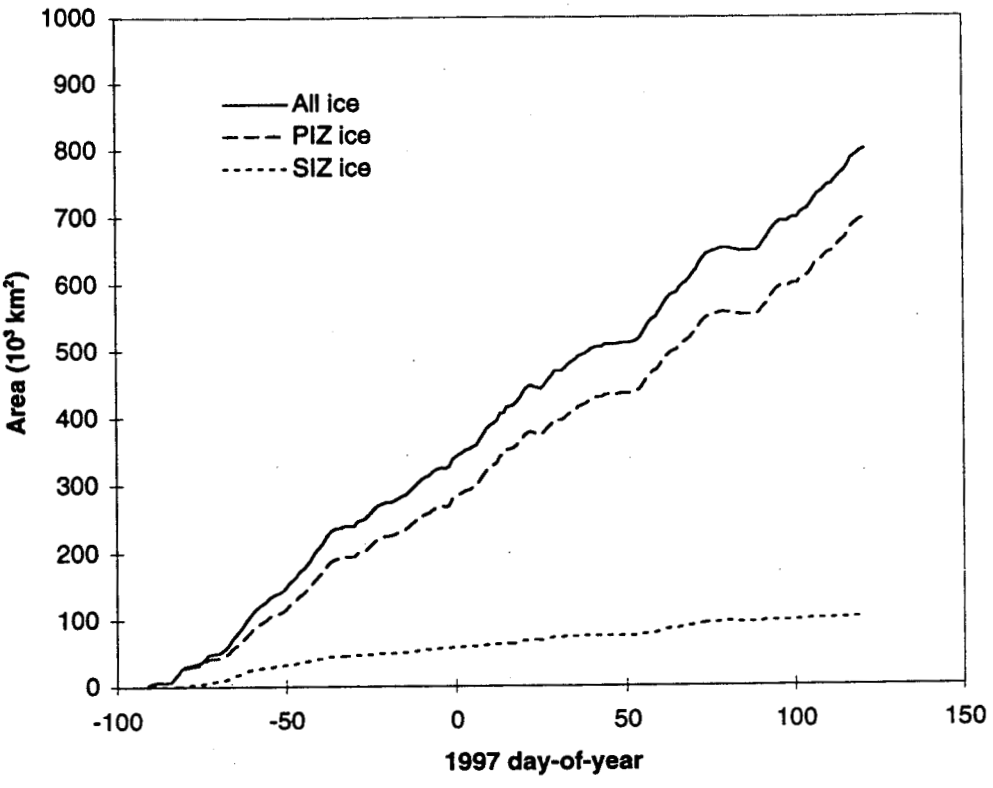
All ice
PIZ ice
SIZ ice
Area (10^3 km^2)
1000
900
800
700
600
500
400
300
200
100
0
-100
-50
0
50
100
150
1997 day-of-year

Fig. 7

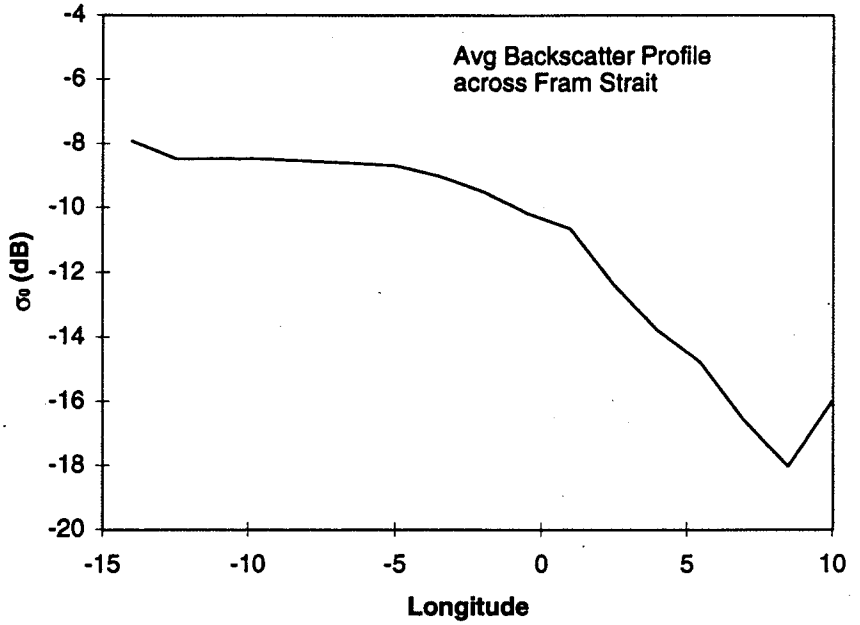
Avg Backscatter Profile
across Fram Strait
-4
-6
-8
-10
-12
-14
-16
-18
-20
σ0 (dB)
-15
-10
-5
0
5
10
Longitude

Fig. 8

Fig. 9

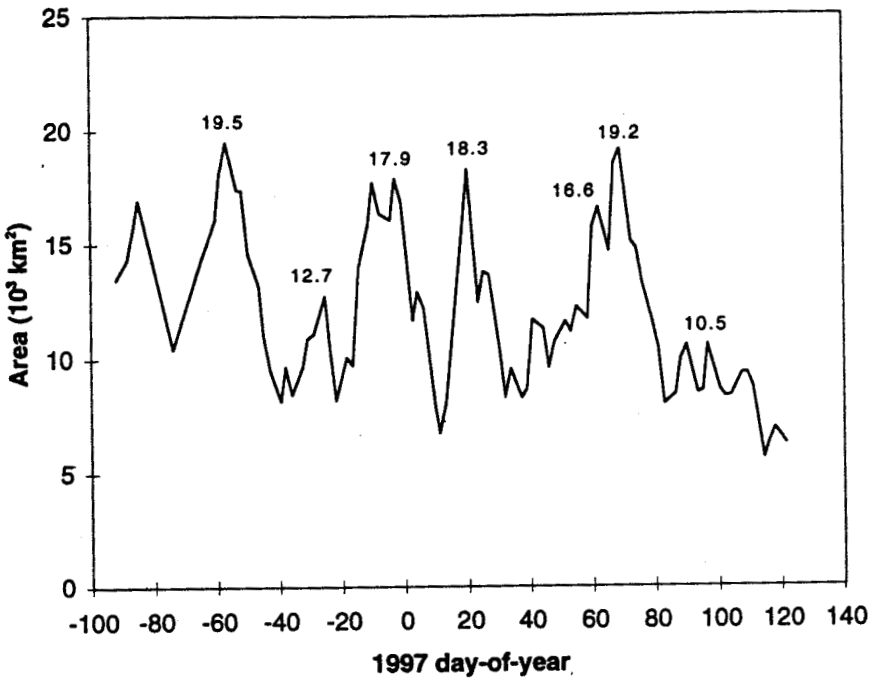
25
20
15
10
5
0
Area (10^3 km^2)
19.5
12.7
17.9
18.3
16.6
19.2
10.5
-100 -80 -60 -40 -20 0 20 40 60 80 100 120 140
1997 day-of-year

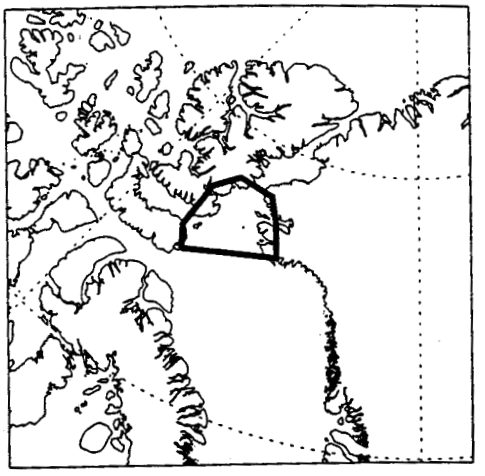

Fig. 10

Fig. 11

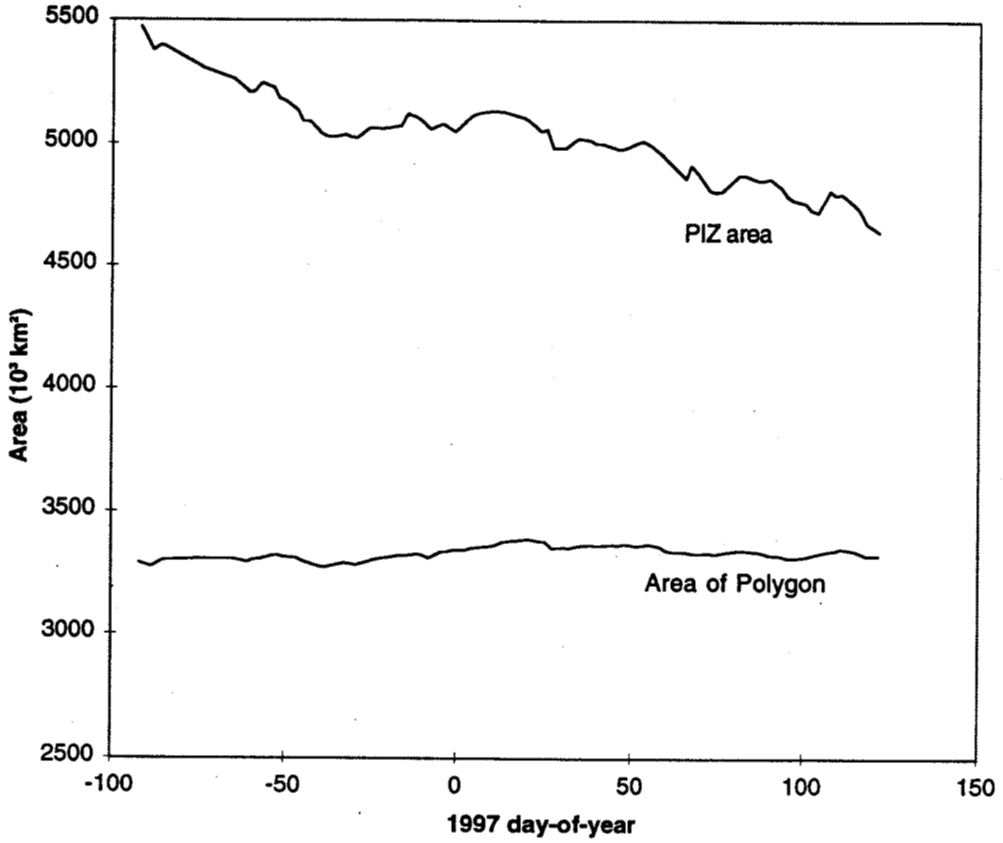
5500
5000
4500
4000
3500
3000
2500
Area (10³ km²)
PIZ area
Area of Polygon
-100
-50
0
50
100
150
1997 day-of-year

Fig . 12